Materials Today Bio 28 (2024) 101217

Contents lists available at ScienceDirect

Materials Today Bio

journal homepage: www.journals.elsevier.com/materials-today-bio

Bionic aggregation-induced emission photosensitizer for enhanced cancer immunotherapy

Zhongxian Chen [a,1], Zeming Liu [c,1], Yingguang Zhou [a,e,1], Kexiang Rao [a], Jiaxin Lin [d], Daoming Zhu [a,*], Shipeng Ning [d,**], Hongbin Wang [b,***]

[a] Department of General Surgery, Guangdong Provincial Key Laboratory of Precision Medicine for Gastrointestinal Tumor, Nanfang Hospital, Southern Medical University, Guangzhou, Guangdong, 510515, China
[b] The Second Ward of Breast Surgery, Cancer Hospital Affiliated to Harbin Medical University, Harbin, 150000, China
[c] Department of Plastic Surgery, Tongji Hospital, Tongji Medical College, Huazhong University of Science and Technology, Wuhan, 430030, China
[d] Department of Breast Surgery, The Second Affiliated Hospital of Guangxi Medical University, Nanning, 530000, China
[e] Department of Orthopaedic Surgery, The Fifth Affiliated Hospital, Southern Medical University, Guangzhou, Guangdong, 510515, China

ARTICLE INFO

Keywords:
Cold exposure therapy
Aggregation-induced emission photosensitizer
GSH depletion
Type I PDT
Cancer immunotherapy

ABSTRACT

Cold exposure therapy (CE), as an inexpensive method, has shown great potential in cancer therapy. Exploring the combined anti-tumor mechanism of CE and traditional therapies (such as photodynamic therapy (PDT)) is exciting and promising. Here, a bionic aggregation-induced emission photosensitizer system (named THL) is designed for combined CE to enhance anti-tumor immunotherapy. THL inherits the homologous targeting ability of tumor derived exosomes, promoting the enrichment of THL at the tumor site. Under external illumination, THL generates hydroxyl radicals and superoxide anions through type I PDT. In addition, mice are pretreated with cold exposure, which promotes THL mediated PDT and reactive oxygen species (ROS) generation by reducing the production of ATP and GSH in tumor tissue. This combination therapy increases production of ROS within the tumor, inhibits the growth of distant tumors, recurrent and rechallenged tumors and increases the number of cytotoxic CD8+T cells and memory T cells. Compared to PDT alone, combination therapy shows greater advantages in tumor immunotherapy. The combination therapy strategy provides new ideas for cancer immunotherapy.

1. Introduction

Previous studies show that tumors have unique metabolic characteristics, which can produce adenosine triphosphate (ATP) through and provide energy for cellular activities [1]. For this reason, tumor cells are extremely dependent on glucose and will consume a large amount of glucose from the body, providing energy for their growth and metastasis [2,3]. Glucose is an accomplice to the rampant proliferation of tumor cells in the body, but it can also become a breakthrough point for people to explore anti-cancer strategies. Recently, Cao et al. revealed a novel strategy to activate brown fat and inhibit solid tumor growth through cold stimulation [4]. This study found that cold exposure therapy (CE) activates brown adipose tissue (BAT) in mice, thereby promoting glucose uptake by brown adipose tissue, while inhibiting glucose uptake by tumor cells. Cold activated brown adipose tissue effectively inhibits tumor growth by limiting the source of glucose and weakening the tumor's ability to uptake glucose through a blood glucose competition mechanism and has been validated in various mouse tumor models. This CE strategy opens a new mode of tumor treatment, and the treatment results show that the hypoxia situation at the tumor site is alleviated, and the production of ATP in tumor neovascularization and cancer cells is reduced. This leads us to think of combining cold exposure therapy with type I photodynamic therapy (PDT) to produce a therapeutic effect of "1 + 1>2". Exploring the combined anti-tumor mechanism of CE and traditional therapies (such as photodynamic therapy) is exciting.

In recent years, nanotechnology, nanomedicine and PDT has

* Corresponding author.
** Corresponding author.
*** Corresponding author.
E-mail addresses: zhudaoming666@smu.edu.cn (D. Zhu), nspdoctor@sr.gxmu.edu.cn (S. Ning), wanghongbin@hrbmu.edu.cn (H. Wang).
[1] Authors contributed equally.

https://doi.org/10.1016/j.mtbio.2024.101217
Received 16 June 2024; Received in revised form 8 August 2024; Accepted 23 August 2024
Available online 24 August 2024

received extensive research [5–14]. Especially for PDT based on aggregation-induced emission (AIE) photosensitizers. AIE molecules can resist photobleaching, and have significant advantages over traditional aggregation cause quenching (ACQ) photosensitizers [15–23]. In addition, type I AIE photosensitizers can generate reactive oxygen species (ROS) such as hydroxyl radicals (•OH) and superoxide anions ($\bullet O_2^-$) under hypoxic conditions, overcoming the limitations of the tumor hypoxic microenvironment [24]. However, reducing substances such as glutathione, which are highly expressed in the tumor microenvironment, can clear reactive oxygen species and protect tumor cells from damage [25]. Currently, a large number of researchers conduct tumor treatment by combining PDT and glutathione (GSH) consumption strategies [26]. GSH is formed by peptide bond condensation of glutamic acid, cysteine, and glycine. L-glutamic acid and L-cysteine are catalysed by γ-glutamylcysteine synthase to produce γ-glutamylcysteine (γ-GC) which is then condensed with glycine by GSH synthase to form GSH [27]. Both synthesis steps require the involvement of ATP [28]. Based on this, we come up with the idea of combining CE with type I AIE photosensitizers to achieve efficient tumor treatment.

Here, we construct a bionic aggregation-induced emission photosensitizer system (named THL) for combined CE therapy to explore the mechanism of combined therapy and enhance anti-tumor immune research (Scheme 1). We firstly prepared an AIE photosensitizer TTMN, and then prepared TTMN loaded liposome nanoparticles (TL) through thin film hydration method. Finally, tumor derived exosomes (EXO) and TL are co-extruded to obtain THL. THL inherits the homologous targeting ability of tumor derived exosomes [29,30], promoting the enrichment of THL at the tumor site. Under external illumination, THL can generate •OH, $\bullet O_2^-$ and singlet oxygen ($^1O_2$). In addition, mice were pretreated with CE, which reduced the levels of glucose, ATP, and GSH at the tumor site and enhanced THL mediated PDT and reactive oxygen species generation. We validated the therapeutic effect of THL combined with CE using bilateral tumor mouse models and recurrence tumor models. The results showed that this combination therapy inhibited the growth of distant tumors, recurrent and rechallenge tumors, enhanced tumor immunogenic cell death (ICD), promoted dendritic cells (DCs) maturation, and increased the number of cytotoxic CD8+T cells and memory T cells. Compared to THL mediated PDT therapy alone, combination therapy has shown greater advantages in tumor immunotherapy. CE is an inexpensive tumor treatment model with good clinical application prospects. The combination therapy strategy we designed opens a new paradigm of PDT and provided new ideas for tumor immunotherapy.

2. Results and discussion

2.1. Preparation and characterization of THL

The aggregation-induced emission (AIE) molecule TTMN was prepared according to the literature [31]. The relevant characterizations were shown in Figs. S1–S3. TTMN showed obvious AIE characteristics (Fig. S4) and little change in absorption before and after illumination (Fig. S5), which can prevent it from being bleached by light. TTMN loaded liposomes (TL) and TTMN loaded exosomes fused liposomes (THL) were prepared by thin film hydration method. As shown in Fig. 1A, TL showed a distinct liposome vesicle structure, with relatively uniform sizes. The morphological structure of THL was like that of liposomes. As shown in Fig. 1B, the zeta potential of THL was approximately −14.8 mV, which is lower than the zeta potential of TL (approximately −10.1 mV), possibly due to the introduction of EXO membrane protein. The PDI of TL and THL are 0.162 and 0.187, respectively. THL can stably exist in PBS and FBS (Fig. 1C) and has good stability. The western blot experiment indicates that both CD63 and CD9 proteins both exist in THL (Fig. 1D). The proteins on exosomes can directly target tumor cells [18,32], so THL may have good tumor cell targeting ability. The UV visible absorption spectrum of THL shows the appearance of an absorption peak for TTMN, indicating that TTMN has been successfully loaded. The drug loading efficiency of TTMN and EXO protein are determined to be 85.32 ± 3.26 % and 97.03 ± 2.26 % by the standard curve and BCA Protein Assay Kit. Laser confocal scanning microscopy (CLSM) is used to observe the phagocytosis of tumor cells towards TL and THL. After incubation with tumor cells for 1 h, the fluorescence intensity of DiO in the THL group was stronger than that in the TL group (Fig. 1F and G)., indicating that THL can adhere to tumor cells in a short period of time. We tested the ability of TTMN and THL to produce reactive oxygen species (ROS) under light irradiation using

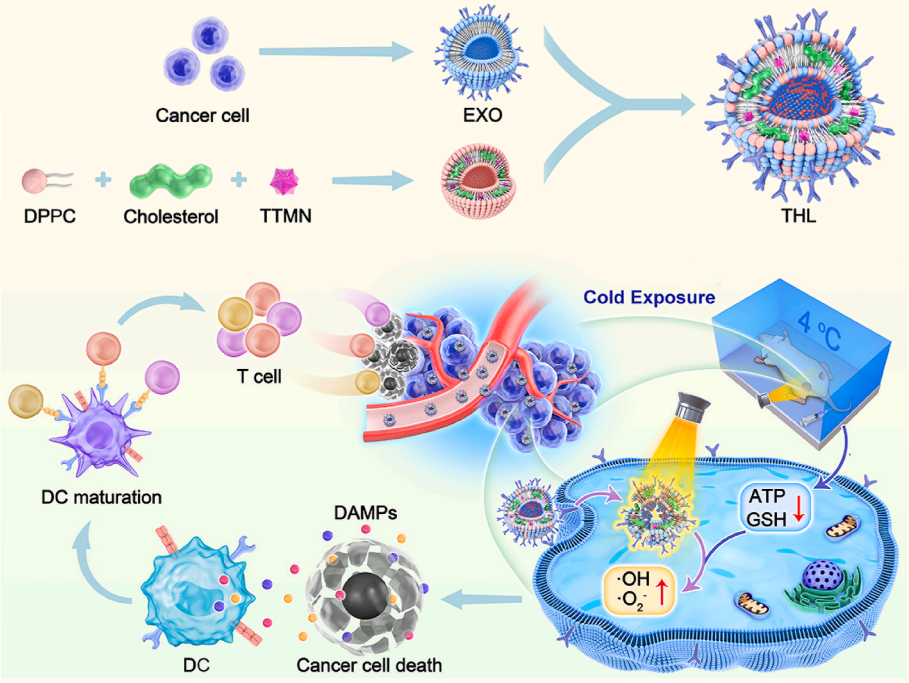

Scheme 1. Schematic illustration of bionic aggregation-induced emission photosensitizer for enhanced immunotherapy of breast cancer.

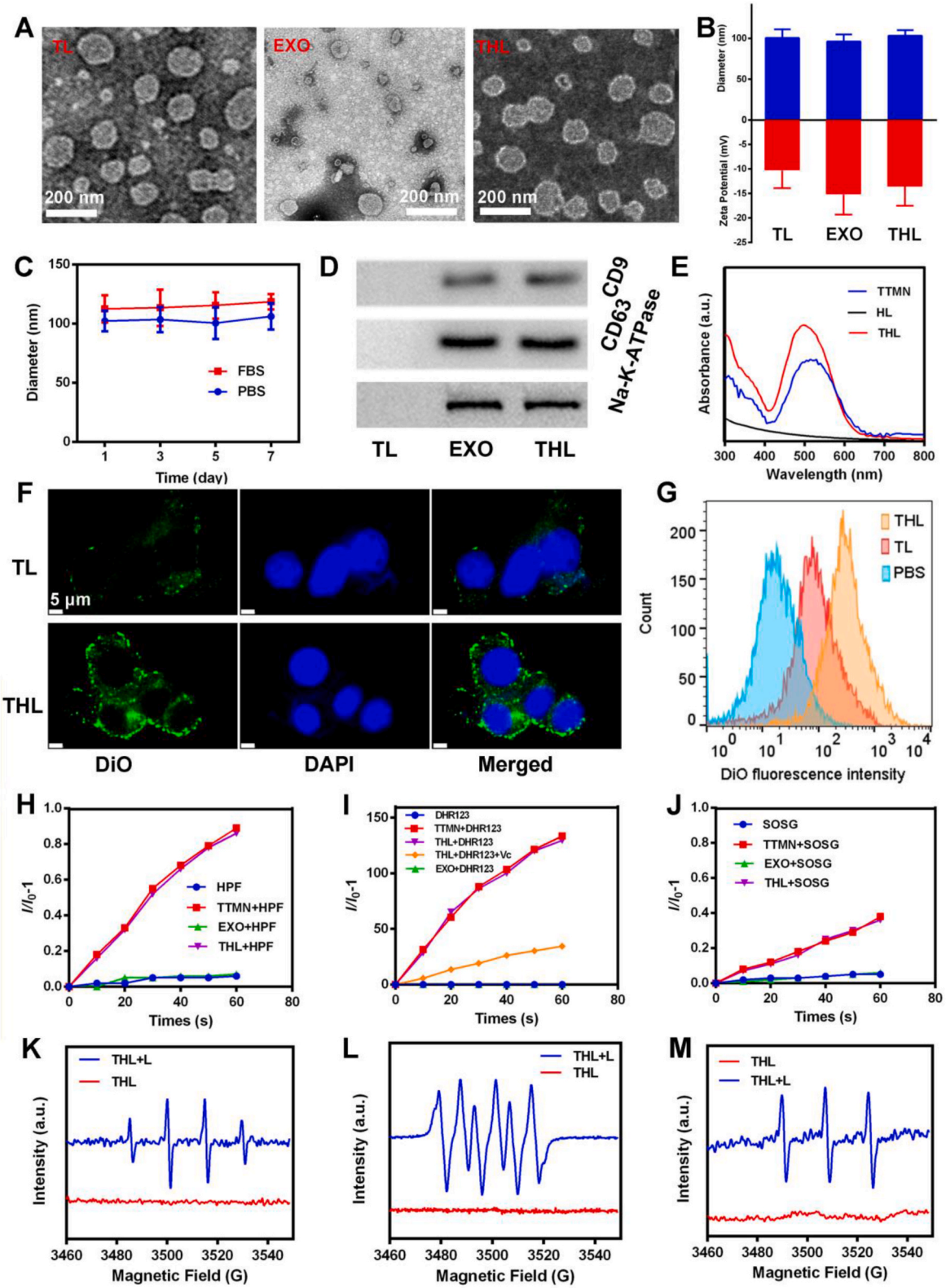

Fig. 1. Preparation and characterization of THL. (A) TEM images of TL, EXO and THL. (B) The hydrodynamic diameter and zeta potential of different formulations suspended in PBS. Data are displayed as the mean ± SD (n = 3). (C) Stability of THL in PBS or PBS containing 10 % FBS. Data are displayed as the mean ± SD (n = 3). (D) EXO markers, including CD63 and CD9, were detected using western blotting. (E) Absorption spectra of chloroperoxidase (in PBS), THL (in PBS), blank EXO hybrid liposomes (HL, in PBS) and TTMN (DMSO). (F) CLSM images of cancer cells incubated with DiO labelled TL or THL for 1h. Blue: DAPI; Green: DiO. (G) The frequency of different DiO fluorescence intensities appearing in Fig. 1F (measured by Zen software). (H) Relative changes in fluorescence intensity of HPF, (I) DHR123 and (J) SOSG after indicated treatments under white light irradiation. Light power: 10 mW/cm^2. (K) Generation of •OH, (L) $•O_2^-$ and (M) $^1O_2$ by the THL was determined by ESR. L: White Light, 10 mW/cm^2.

HPF, DHR123, SOSG and Electron Paramagnetic Resonance (EPR). As shown in Fig. 1H–M, TTMN and THL produced •OH, $\bullet O_2^-$ and $^1O_2$ under light irradiation, indicating the existence of type I and type II properties. Overall, we have successfully prepared THL, which can target tumor cells well and have good ability to produce ROS.

2.2. In vitro anti-tumor ability of THL

In view of the excellent photophysical properties of THL, we further explored the killing effect of THL on 4T1 breast cancer cells *in vitro*. To simulate the glucose reduction in tumor tissue induced by cold exposure therapy, we cultured tumor cells *in vitro* using a low-glucose treatment (LG). Firstly, DCFH-DA fluorescent probe was used to detect the ROS levels in 4T1 cells after different treatments. As shown in Fig. 2A and B, under normoxic conditions, compared to the PBS + L group, the LG group only showed weak green fluorescence. In contrast, the THL + L and TL + L + LG groups showed bright intracellular green fluorescence, while the THL + L + LG group exhibited the most significant fluorescence. These results indicated that THL mediated PDT and low glucose can induce ROS generation. As is well known, hypoxia is a major characteristic of the malignant tumor microenvironment [23,33]. Most existing PDT systems are highly dependent on oxygen concentration, and type I photosensitizers have relatively low oxygen dependence and can maintain ROS production ability in severely hypoxic tumor sites [17,34]. Subsequently, we investigated the tumor killing effect of the THL system under hypoxic conditions. As shown in Fig. 2C and D, under hypoxic conditions, compared to other control groups, the THL + L + LG group exhibited the brightest green fluorescence, further indicating that THL mediated PDT and low glucose combined therapy can also ensure higher ROS production under hypoxic conditions. Subsequently, further research was conducted on how THL affects glucose metabolism within tumor cells. As shown in Fig. 2E and F, THL + L + LG reduced intracellular ATP and GSH production. As mentioned earlier, the synthesis of GSH requires the involvement of ATP, which is also the main reason why LG led to the downregulation of GSH.

Given the excellent ROS production ability and ATP inhibition of the THL, we next investigated the killing ability of THL on 4T1 cells. As shown in Fig. 2G, compared to the PBS group, LG therapy caused partial tumor cell killing, which was due to low glucose therapy causing intracellular ATP consumption. The killing effect of THL + L group reached about 40 %, which was due to THL mediated PDT and damage to tumor cells. Compared to TL + L + LG, THL + L + LG had a more significant killing effect, with a cell survival rate of less than 10 %. The combination of PDT and LG resulted in a therapeutic effect of "1 + 1>2". These results indicated that THL + L + LG had a good tumor cell killing effect, and the killing effect is concentration dependent (Fig. 2H). The results of flow cytometry apoptosis shows that THL + L + LG led to earlier and late-stage apoptosis (Fig. 2I). In addition, THL had low toxicity to macrophage cells, demonstrating good safety (Fig. S6).

2.3. In vitro induction of immunogenic cell death (ICD)

ICD is considered a special form of cell death that can release tumor associated antigens, including apoptotic body, damaged DNA fragments, and damage associated molecular patterns (DAMPs), and help trigger specific immune responses in hosts with strong immunity [5,35–37]. According to reports, ICD effects can promote the release of DAMPs in dying tumor cells, including endoplasmic reticulum chaperone calcium reticulum protein (CRT), adenosine triphosphate (ATP), and high mobility cassette 1 (HMGB1) [38–40]. Subsequently, antigen-presenting cells (APCs), including DC, will be activated to present tumor antigens and ultimately stimulate immune responses against the tumor [41]. Next, we investigated whether the synergistic therapeutic effect of THL can induce immunogenic cell death (ICD) in 4T1 cells. As shown in Fig. 3A and B, compared to the PBS + L group and LG group, the cells treated with TL + L show slight expression of CRT, while TL + L + LG show moderate expression. THL + L + LG treatment significantly promoted the expression of CRT. In addition, as shown in Fig. 3C and D, the cancer cells treated with THL + L + LG release the highest amount of HMGB1. This indicated THL mediated PDT combined with LG treatment can induce effective ICD in cancer cells, which is beneficial for tumor immunotherapy. As shown in Fig. S7, combination therapy significantly induced lipid peroxidation in tumor cells, indicating the occurrence of ferroptosis. There are many studies indicating that the iron death pathway can induce ICD and release DAMPs [42–44]. Therefore, the combination therapy induced ICD may be achieved through ferroptosis. The therapeutic mechanism of THL + L + LG was further studied by detecting dendritic cells (DCs) through Transwell experiments and flow cytometry. DCs plays a crucial role in immune response [45]. T lymphocytes can bind to co-stimulatory molecules to induce T cell-mediated immune responses [40]. As shown in Fig. 3E and F, the percentage of mature DCs in the THL + L + LG group was 57.6 %, which was 1.32 times higher than that in the TL + L + LG group and increased by 2.76 times compared to the control group. In summary, our experimental results indicated that THL mediated type I PDT combined with LG induces the occurrence of ICD in tumor cells.

2.4. In vivo anti-tumor ability of THL

Next, further studies were conducted on the *in vivo* therapeutic outcomes of the system. Prior to this, the pharmacokinetics and biological distribution of TL and THL were measured by HPLC method (Fig. 4A and B). THL has longer blood circulation time and better tumor targeting than TL. Then, we investigated the changes in adipose tissue after CE treatment. Brown adipose tissue (BAT) was dissected and stained with Uncoupling protein 1 (UCP1) after CE treatment. UCP1 is a mitochondrial carrier protein located in the inner membrane of mitochondria and a key protein in non-shivering thermogenesis (NST) [46]. The results indicated an increased UCP1 expression in BAT, suggesting an increased heat production in BAT (Fig. 4c and D). In warm environments, the main function of white adipose tissue (WAT) is to store energy and expand and contract according to metabolic conditions [47]. Under environmental stimuli, WAT undergoes phenotype and metabolic reprogramming to become brown like tissue [46]. The BAT in the xenograft tumour-bearing mice exhibited highly dense structures under CE, which appeared as smaller multilocular structures (Fig. 4E), a typical morphological phenotype for BAT activation. Glucose-tolerance tests showed a quick glucose clearance under cold exposure in the xenograft tumour models (Fig. S8). These experiments demonstrated that cold exposure significantly decreases blood glucose levels in tumour-bearing mice. The ATP content in BAT significantly increased (Fig. S9).

Next, we conducted an anti-tumor study of THL. We found through preliminary experiments that the optimal treatment combination was TTMN dose of 5 mg/kg and CE treatment time from day 0 to day 5 (Figs. S10A and S10B). Moreover, injection of 4T1 cells derived exosomes (EXO) or THL alone had no inhibitory effect on tumor growth, and there was no significant difference in tumor infiltration of $CD8^+$ T cells (Figs. S10C and S10D). These results indicated that there is no potential immune response for EXO or THL alone. As shown in Fig. 5A, we inoculated 4T1 cells into the right leg of mice as the primary tumor. When the tumor on the right side reached about 100 mm^3, the mice were randomly divided into 5 groups (5 in each group) and subjected to the following treatments at a specified time: (1) PBS + L; (2) CE; (3) THL + L; (4) TL + L + CE; (5) THL + L + CE. The environmental temperature for CE treatment is 4 °C, and mice that have not been treated with CE are placed at 25 °C. After the end of treatment on the 5th day, 4T1 cells were implanted on the opposite side as distal tumors. Another group of mice were euthanized on the 8th day and the glucose, ATP and GSH contents in the tumor tissues of each group of mice were measured (Fig. 5B and C and S11).The results showed a partial decrease in glucose and GSH content in the tumor tissue of the CE group, which most intuitively

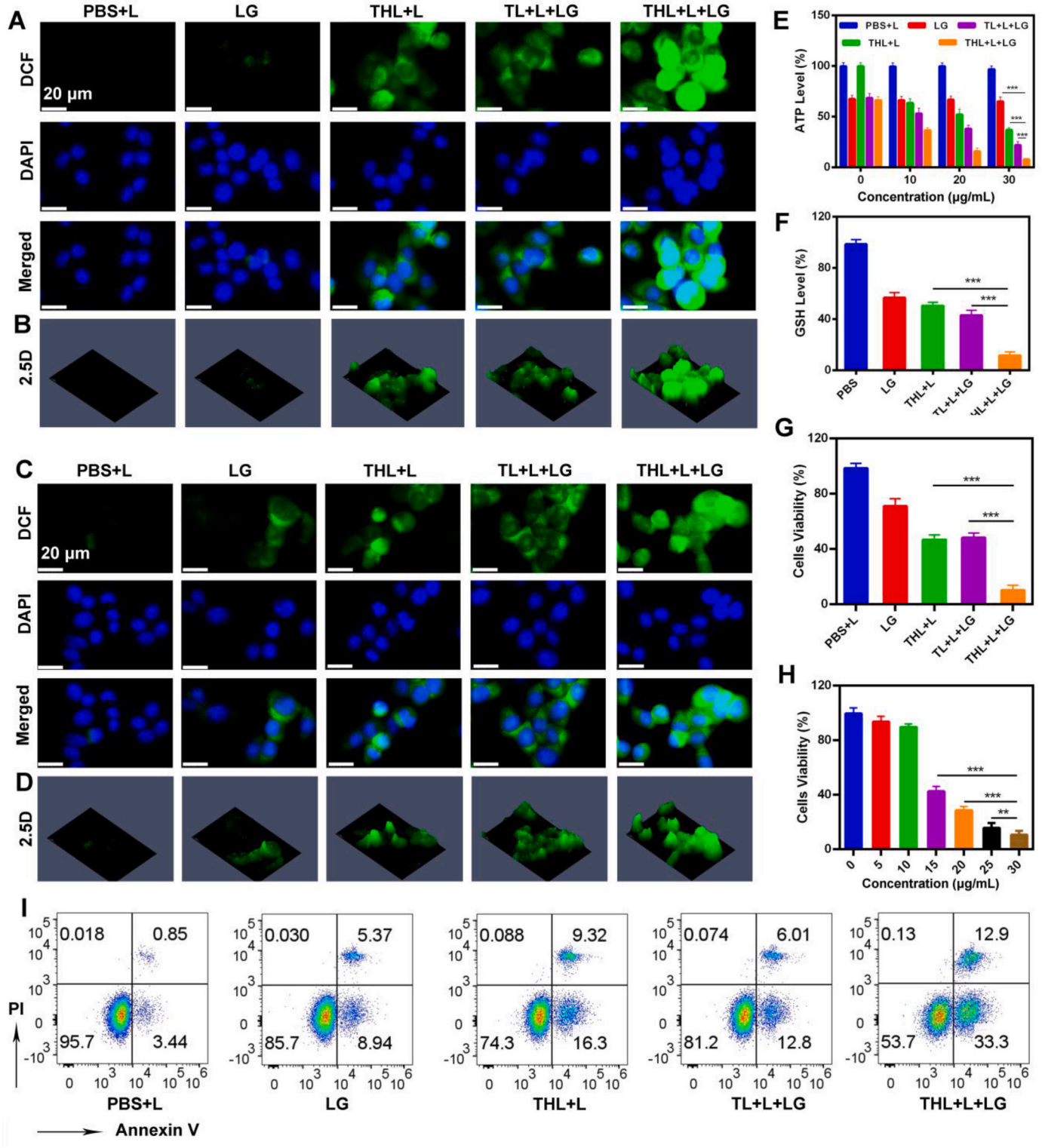

Fig. 2. *In vitro* anti-tumor evaluation. (A) Fluorescence images of ROS generation in normoxic 4T1 cells pretreated with indicated formulations, and (B) the corresponding 2.5D images of different DCFH-DA (DCF) intensities appearing in Fig. 2A (measured by Zen software). LG: low-glucose treatment. L: 0.01 W/cm^2, 5 min. The TTMN concentration was 30 μg/mL. (C) Fluorescence image of ROS generation in hypoxic 4T1 cells pretreated with indicated formulations, and (D) the corresponding 2.5D images of different DCFH-DA (DCF) intensities appearing in Fig. 2C (measured by Zen software). L: 0.01 W/cm^2, 5 min. The concentration of TTMN is 0.03 mg/mL. (E) Intracellular ATP and (F) GSH levels after indicated therapy. The concentration of TTMN is 0.03 mg/mL. (G) Cell viability of 4T1 cells after different treatments (n = 3). L: 0.01 W/cm^2, 5 min. The concentration of TTMN is 0.03 mg/mL. (H) Cell viability of 4T1 cells after THL + L treatments with different TTMN concentration (n = 3). L: 0.01 W/cm^2, 5 min. (I) Annexin V/PI assy by flow cytometry after various treatments in 4T1 cells. The concentration of TTMN is 0.03 mg/mL. Statistical significance was calculated via one-way ANOVA with Tukey's test: **p < 0.01, ***p < 0.001.

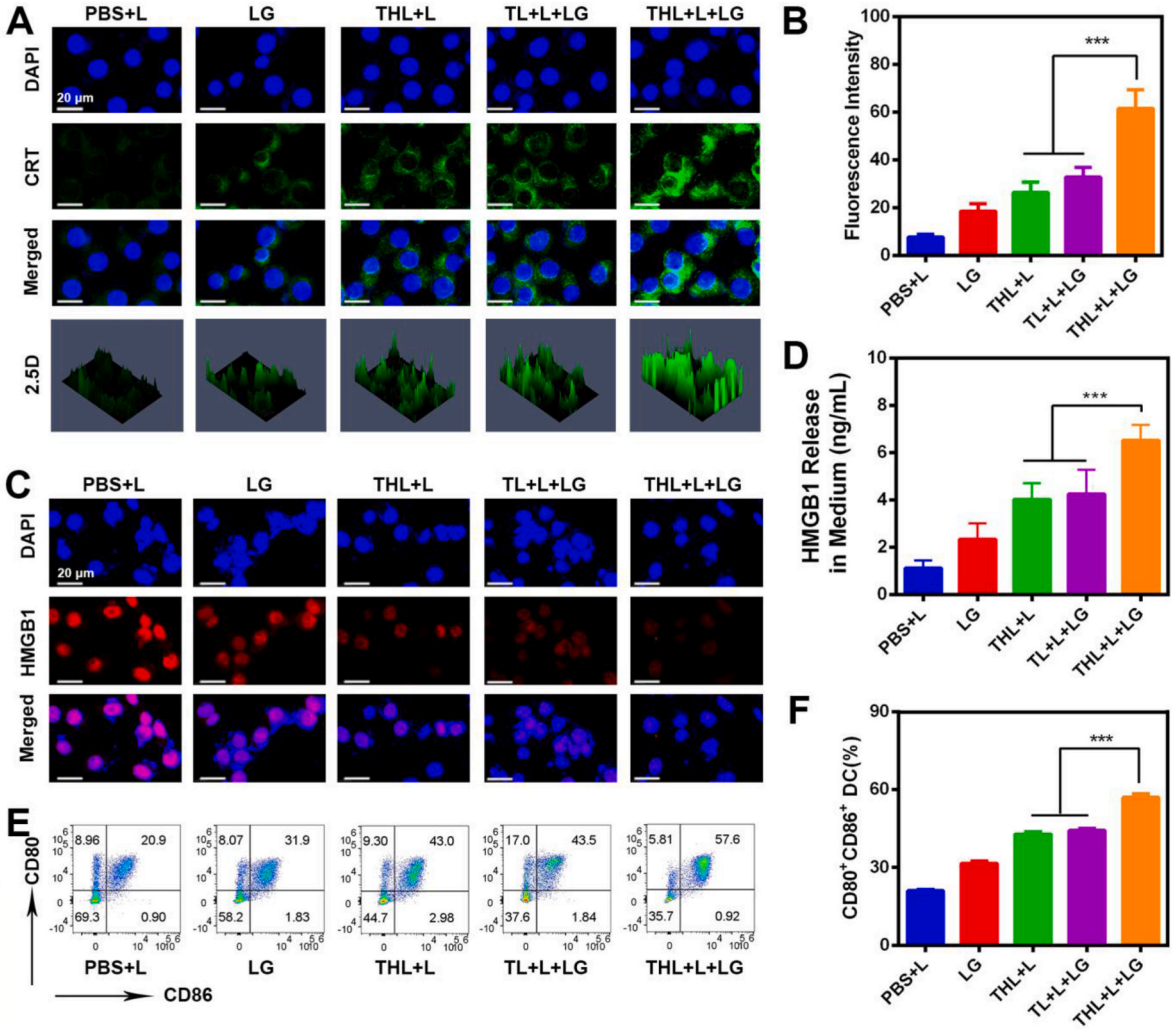

Fig. 3. Inducing immunogenic cell death (ICD) *in vitro*. (A) Fluorescence images of calreticulin (CRT) in 4T1 cells treated with indicated formulations, and the corresponding 2.5D images of different CRT intensities appearing in Fig. 3A (measured by Zen software). LG: low-glucose treatment. L: 0.01 W/cm^2, 5 min. The TTMN concentration was 30 μg/mL. (B) The corresponding CRT fluorescence intensity in Fig. 3A (measured by FlowJo software). (C) Immunofluorescence staining (Red: HMGB1, Blue: DAPI) in 4T1 cells after various treatments. (D) Quantitative examination of released HMGB1 from 4T1 cells after various treatments (n = 3). (E) Matured DCs (CD80+CD86$^+$) measured by flow cytometry and (F) quantitative analysis (n = 3). Data are shown as the mean ± SD. The concentration of TTMN in above experiments is 0.03 mg/mL. Statistical significance was calculated via one-way ANOVA with Tukey's test: ***p < 0.001.

demonstrated the effect of CE on glucose in tumor tissue. The glucose concentration and GSH content in the THL + L + CE group significantly decreased, possibly due to further exacerbation of cell metabolism inhibition caused by photodynamic therapy. In addition, the production of ROS in tumor tissue was shown in Fig. S12. THL mediated type I PDT combined with CE had the strongest DCF fluorescence, indicating that the THL system induced ROS generation *in vivo*. The primary and distant tumors in the PBS + L group produced rapidly, and on the 21st day after treatment, the tumor volume expanded to 843.6 mm^3 and 332.6 mm^3, respectively (Fig. 5D and E). As shown in Fig. 5F and Fig. S13, the TL + L + CE group had an inhibitory effect on the growth of both primary and distance tumors. It was worth noting that TL + L + CE cannot target tumor cells, which greatly limited its anti-tumor effect in tumor tissue. In addition, we also monitored the survival rate of mice. The PBS + L group, CE group, TL + L + CE group, and THL + L group mice all died within 60 days (Fig. 5G), while the THL + L + CE group extended the lifespan of mice, achieving a survival rate of 80 % at 60 days, demonstrating good therapeutic effects.

To further evaluated the induction of tumor tissue ICD and DCs maturation by the THL + L + CE group, we collected mouse tumor tissue. The results of tumor immunofluorescence staining analysis showed that the THL + L + CE group had the highest proportion of CRT expression (Fig. 5H). The DCs in the lymph node and primary tumors were co-stained with CD80 and CD86 antibodies, and the proportion of mature DCs was detected using flow cytometry. Consistent with previous *in vitro* experimental results, the proportion of mature DCs in the THL + L + CE group was higher than that in the THL + L group (Fig. 5I–S14 and S15). The HE staining results showed significant damage to the distal tumor tissue treated with THL + L + CE group (Fig. 5J). Since no direct treatment was performed on the distal tumor, the damage to the distal tumor tissue largely represented the immune system's killing effect on the tumor tissue. Enzyme-linked immunosorbent assay (ELISA) was used to determine the concentration of cytokines in serum and evaluate the systemic immune response. Compared with TL + L + CE group and THL + L, the THL + L + CE treatment sustainably promoted TNF- α and IFN- γ secretion (Fig. 5K and L). In addition, tissue immunofluorescence showed an increase in CD8+T lymphocyte infiltration in the distant tumor tissues of mice treated with THL + L + CE group (Fig. 5M). These results indicated that THL + L + CE treatment effectively promoted the infiltration and killing of CD8+T lymphocytes. Further detection of CD4$^+$ and CD8+T lymphocyte ratio in distant tumor tissue using flow cytometry revealed that the THL + L + CE group had a

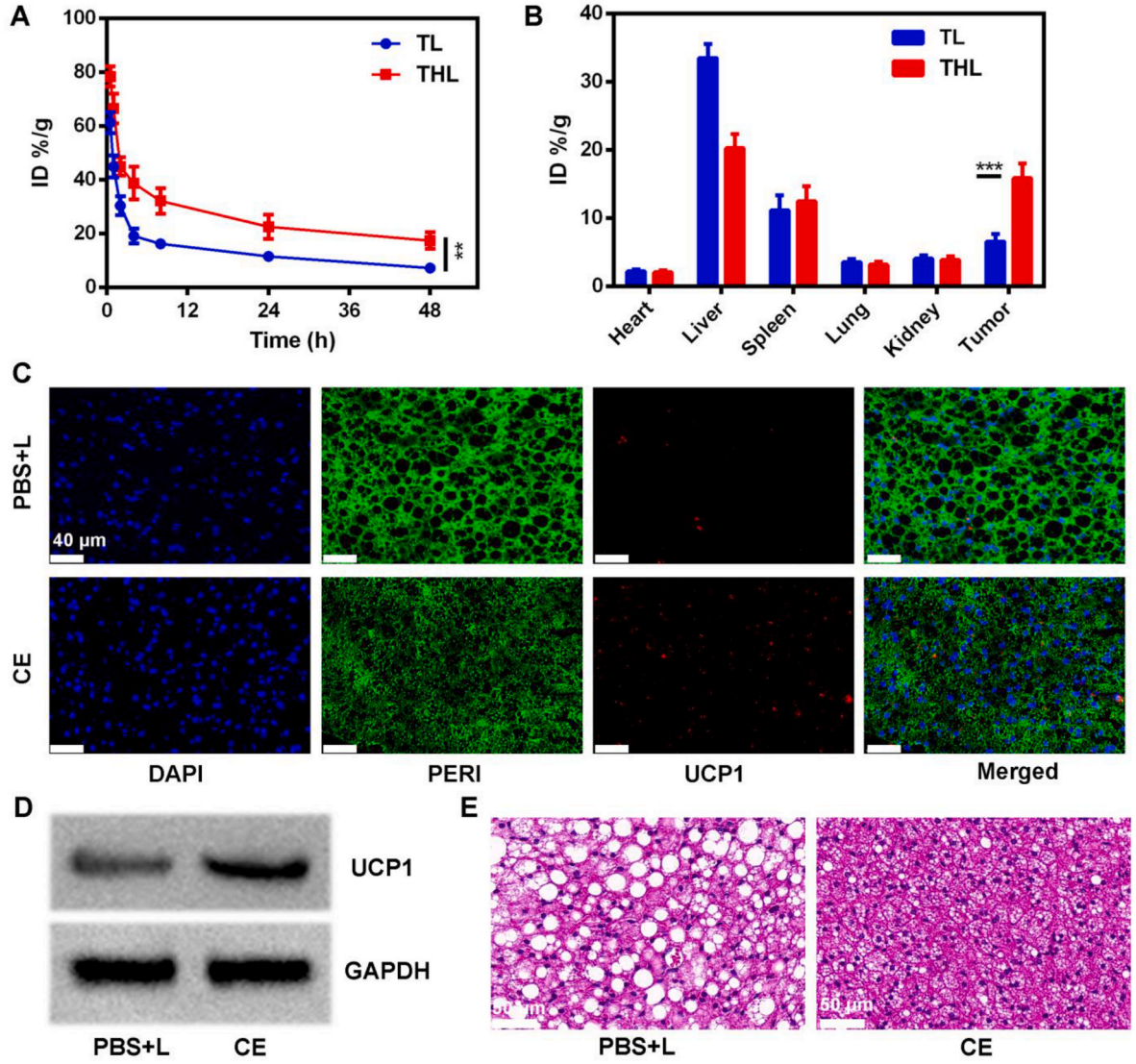

Fig. 4. Tumor targeting and BAT analysis *in vivo*. (A) *In vivo* pharmacokinetic profile of indicated treatment. The dose of TTMN was 5 mg/kg. (B) Biodistribution profile of THL and TL in the main organs and tumor tissues at 12-h post-injection. The dose of TTMN was 5 mg/kg. (C) Immunofluorescence staining of BAT for UCP1 and perilipin, followed by counterstaining with DAPI (blue) in 4T1 tumor-bearing mice under the 25 °C (PBS + L) and 4 °C (CE) conditions. (D) Western blot was used to detect the expression of UCP1 expression in BAT after different treatments. (E) H&E histological staining of BAT after different treatments. Statistical significance was calculated via one-way ANOVA with Tukey's test: **$p < 0.01$.

CD8+T lymphocyte ratio of 28.1 % in distant tumors, which was higher than the THL + L group (19.8 %; Fig. 5N and O). During the treatment cycle, the weight of mice steadily increased (as shown in Fig. S16), and there was no significant damage to liver and kidney function and organs in the experimental and control groups of mice (as shown in Figs. S17 and S18), indicating that the treatment system has good biosafety.

2.5. *In vivo anti-tumor recurrence and rechallenge*

The immune memory effect is one of the important mechanisms for inhibiting tumor recurrence and treatment [48]. To investigate the anti-tumor immune memory effect induced by THL + L + CE, we established another mouse model. After the treatment group mentioned above, the primary tumor on the right side of the mice was removed, and 4T1 cells were re inoculated into the left hind leg (Fig. 6A). As shown in Fig. 6B, the THL + L + CE group of mice still had the longest survival time in this model. The results of tumor volume monitoring (Fig. 6C, D and 6G) showed that the PBS + L group of mice experienced rapid tumor recurrence, while the THL + L + CE group of mice showed an inhibition of tumor recurrence rate. As shown in Fig. 6E and S6, after treatment, the tumor weight in the THL + L + CE group significantly decreased. After tumor surgery, memory T cells can survive for a long time and differentiate and proliferate into killer T cells under the stimulation of new tumor antigens [5]. To evaluate the long-term anti-tumor effect, we investigated the proportion of central memory T cells (TCM) in the peripheral blood of mice in each treatment group. As shown in Fig. 6F and H, the proportion of TCM in the blood after THL + L + CE treatment was about 1.88 times that of the THL + L group and 1.73 times that of the TL + L + CE group. Tissue fluorescence slice analysis showed that after THL + L + CE treatment, the infiltration of CD8+T cells (represented by green fluorescence) increased in rechallenged tumor tissue (Fig. 6I). This indicated that THL + L + CE triggered a strong immune memory response. In summary, we have cleverly designed an anti-tumor system that combines CE. And achieved good therapeutic effects *in vivo*. THL mediated type I PDT combined with CE can effectively stimulate tumor immunity, promote the maturation of lymph node dendritic cells and the infiltration of T lymphocytes. In addition, it effectively inhibited post-operative tumor stimulation and recurrence in mice receiving THL + L

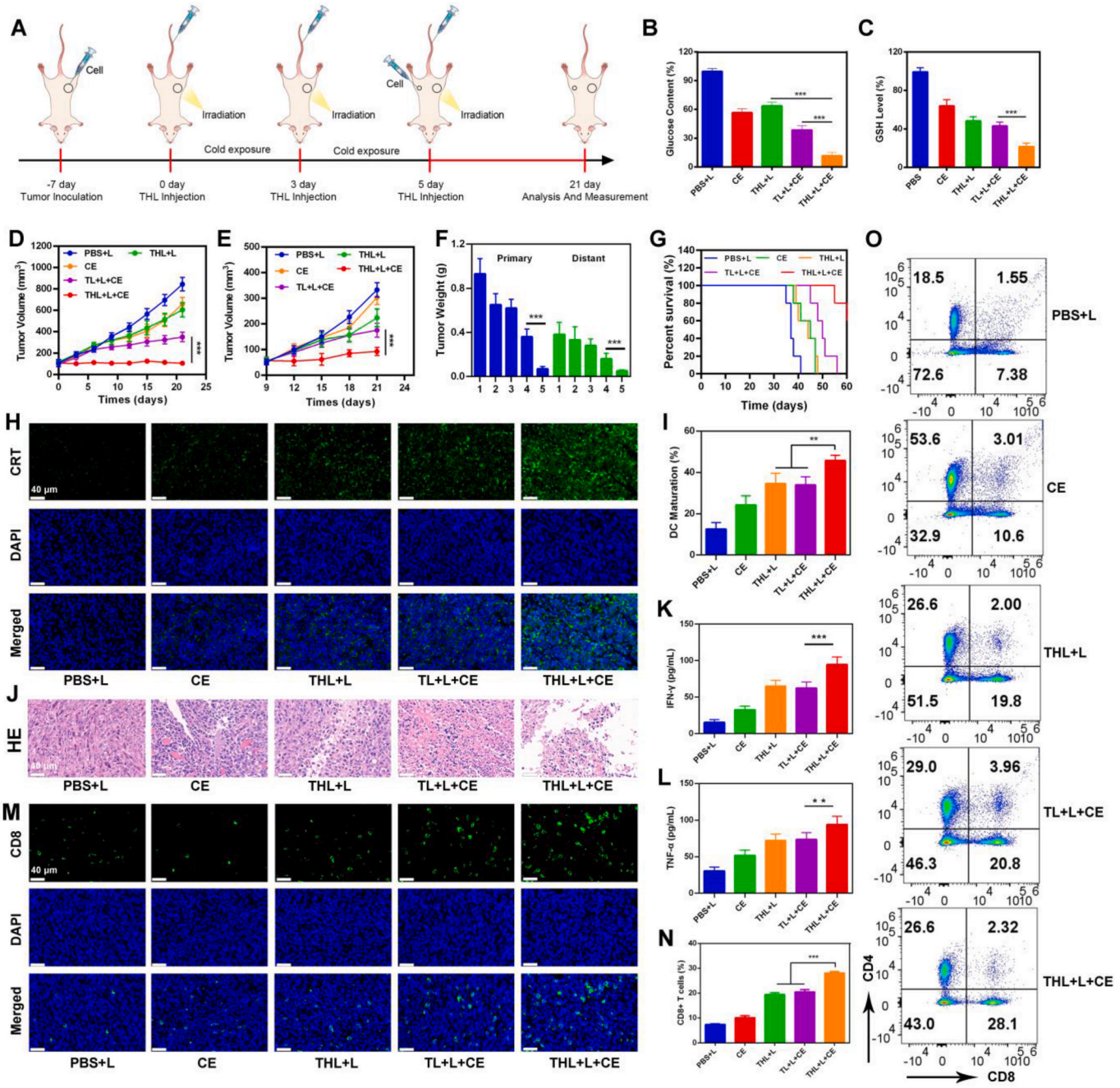

Fig. 5. (A) Schematic illustration of the studies of 4T1 tumor therapy. (B) Detection of glucose and (C) GSH levels in tumors after different treatments. (D) Growth profile of the primary and (E) distant tumor volume after various treatments. (F) Tumor weight of primary and distant tumors. (G) Survival curves after treatment. (H) CRT, staining analyses of primary tumor tissues treated with various treatments. (I) Flow cytometry analysis of treatment-induced dendritic cell maturation in the lymph nodes. (J) HE staining analyses of distant tumor tissues treated with various treatments. (K) ELISA analysis of the levels of proinflammatory cytokines IFN-γ and (L) TNF-α in serum of mice isolated at the end of treatments (n = 5). (M) Immunofluorescence staining of CD8 (green) from distant tumors in different treatment groups. (N) Quantitative analysis and (O) Flow cytometry analysis of $CD4^+$ $CD8^+$ T lymphocytes in distant tumors. The TTMN and EXO protein dosage used in above experimental is 5 mg/kg. Data are shown as the mean ± SD. Statistical significance was calculated via one-way ANOVA with Tukey's test: $^{**}p < 0.01$, $^{***}p < 0.001$.

+ CE. This system has laid a theoretical foundation for clinical application and has great potential for clinical application.

3. Conclusions

In summary, a biomimetic aggregation induced emission photosensitizer system called THL has been successfully prepared. Surprisingly, the homologous targeting ability of THL enabled it to be specifically delivered to tumor tissue and internalized by tumor cells after intravenous injection. Subsequently, under laser irradiation, type I and type II PDT were activated, which had cytotoxic effects on cancer cells. In addition, combined with CE therapy, it not only inhibited glucose uptake by tumor cells and reduced ATP production cancer cells, but also consumed glutathione in tumor cells, thereby enhancing THL mediated PDT and reactive oxygen species (ROS) production. The experimental results indicated that this combination therapy increases the production of ROS within the tumor, inhibits the growth of distant, recurrent, and rechallenged tumors, and increases the number of cytotoxic CD8+T and memory T cells. Compared with PDT alone, combination therapy has shown greater advantages in tumor immunotherapy. This combination

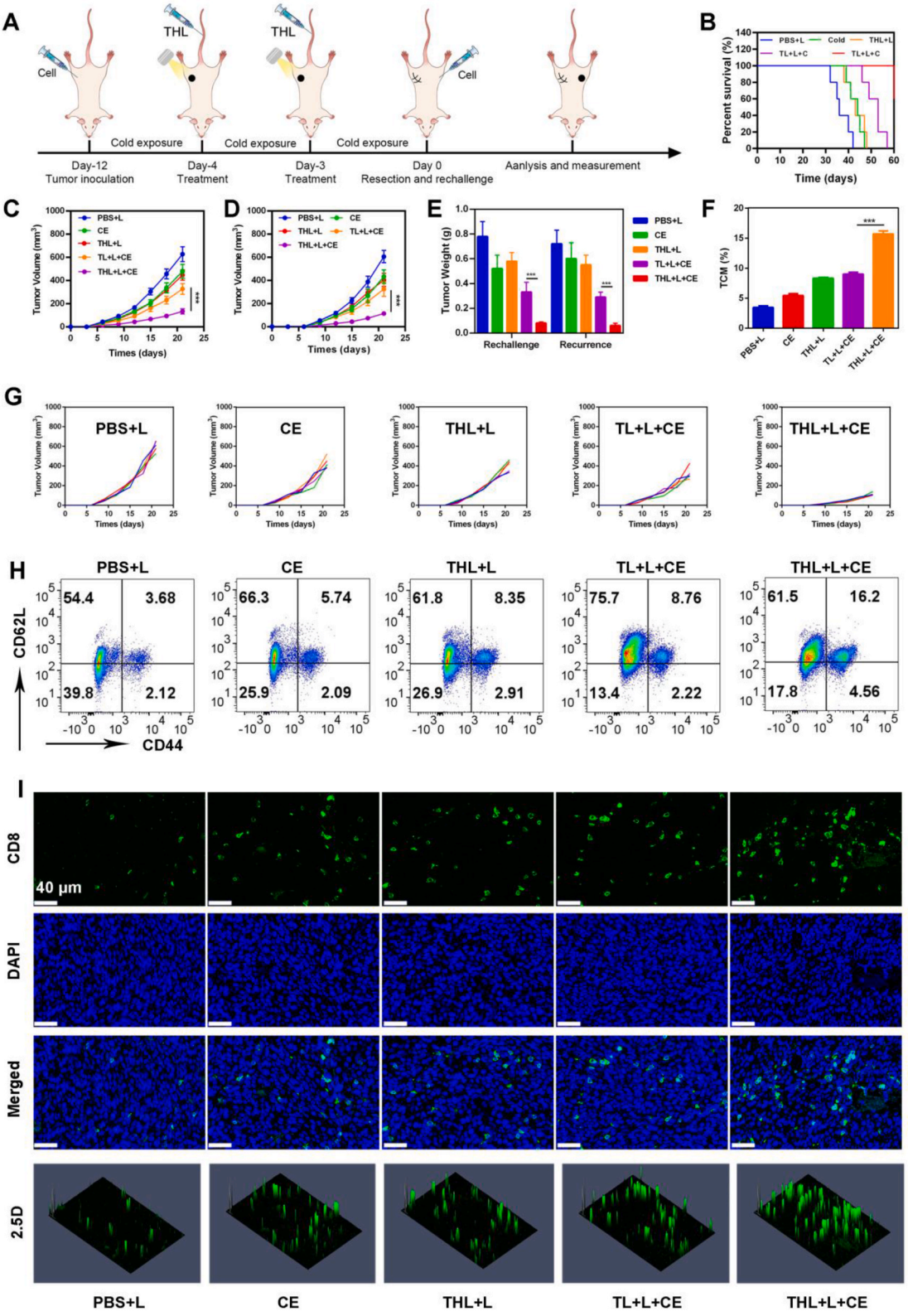

Fig. 6. (A)Schematic illustration of the studies of 4T1 tumor rechallenge and recurrence. (B) Survival curves after treatment. (C) Recurrence of 4T1 tumor growth (n = 5). (D) Rechallenge of 4T1 tumor growth (n = 5). (E) The tumor weight of mice was recorded for various treatments (n = 5). (F) Quantitative statistics of proportion of central memory T cells (TCM cells; CD62L + $CD44^{+}$) in blood on day 21 after the treatment (n = 5). (G) Growth curve of rechallenge tumor in each mouse. (H) Proportion of central memory T cells (TCM cells; CD62L + $CD44^{+}$) in blood on day 21 after the treatment measured by flow cytometry. (I) Immunofluorescence staining analyses of $CD8^{+}$ T cells and the corresponding 2.5D images (measured by Zen software) in rechallenged tumor tissues treated with various treatments. The TTMN and EXO protein dosage used in above experimental is 5 mg/kg. Data are shown as the mean ± SD. Statistical significance was calculated via one-way ANOVA with Tukey's test: ***$p < 0.001$.

therapy strategy provided new possibilities for advancing clinical cancer immunotherapy.

In the future, we will further explore the anti-tumor effects of CE combined with traditional radiotherapy and chemotherapy. In addition, a temperature of 4 °C still has high requirements for clinical treatment and may cause discomfort to patients. Therefore, we will focus on solving the key issue of how to increase the temperature limit of CE therapy to achieve therapeutic effects while reducing side effects.

CRediT authorship contribution statement

Zhongxian Chen: Conceptualization, Data curation, Investigation, Methodology, Software. **Zeming Liu:** Project administration, Investigation, Funding acquisition, Conceptualization. **Yingguang Zhou:** Validation, Resources, Data curation. **Kexiang Rao:** Supervision, Investigation, Formal analysis. **Jiaxin Lin:** Data curation, Investigation, Software. **Daoming Zhu:** Writing – original draft, Supervision, Resources, Conceptualization. **Shipeng Ning:** Writing – review & editing, Validation, Methodology, Conceptualization. **Hongbin Wang:** Writing – review & editing, Software, Project administration, Funding acquisition, Formal analysis.

Declaration of competing interest

The authors declare that they have no known competing financial interests or personal relationships that could have appeared to influence the work reported in this paper.

Data availability

Data will be made available on request.

Acknowledgments

We are grateful for the financial support from the project of improving the basic ability of young and middle-aged teachers in colleges of Guangxi (2023KY0097), the Outstanding Youths Development Scheme of Nanfang Hospital, Southern Medical University (2021J008), the Launch Funding for Talent Introduction of Southern Medical University (R10101041), the GuangDong Basic and Applied Basic Research Foundation (2023A1515011787) and the Science and Technology Projects in Guangzhou (2023A04J2370).

Appendix A. Supplementary data

Supplementary data to this article can be found online at https://doi.org/10.1016/j.mtbio.2024.101217.

References

[1] H.R. Christofk, M.G. Vander Heiden, M.H. Harris, A. Ramanathan, R.E. Gerszten, R. Wei, M.D. Fleming, S.L. Schreiber, L.C. Cantley, The M2 splice isoform of pyruvate kinase is important for cancer metabolism and tumour growth, Nature 452 (7184) (2008) 230. U74.

[2] H. Min, J. Wang, Y. Qi, Y. Zhang, X. Han, Y. Xu, J. Xu, Y. Li, L. Chen, K. Cheng, G. Liu, N. Yang, Y. Li, G. Nie, Biomimetic metal–organic framework nanoparticles for cooperative combination of antiangiogenesis and photodynamic therapy for enhanced efficacy, Adv. Mater. 31 (15) (2019) 1808200.

[3] Z.-X. Chen, M.-D. Liu, M.-K. Zhang, S.-B. Wang, L. Xu, C.-X. Li, F. Gao, B.-R. Xie, Z.-L. Zhong, X.-Z. Zhang, Interfering with lactate-fueled respiration for enhanced photodynamic tumor therapy by a porphyrinic MOF nanoplatform, Adv. Funct. Mater. 28 (36) (2018) 1803498.

[4] T. Seki, Y. Yang, X. Sun, S. Lim, S. Xie, Z. Guo, W. Xiong, M. Kuroda, H. Sakaue, K. Hosaka, X. Jing, M. Yoshihara, L. Qu, X. Li, Y. Chen, Y. Cao, Brown-fat-mediated tumour suppression by cold-altered global metabolism, Nature 608 (7922) (2022) 421–428.

[5] Y. Pan, M. Suo, Q. Huang, M. Lyu, Y. Jiang, S. Wang, W. Tang, S. Ning, T. Zhang, Near-infrared laser-activated aggregation-induced emission nanoparticles boost tumor carbonyl stress and immunotherapy of breast cancer, Aggregate 5 (2023) e432.

[6] J. Xin, C. Deng, M. Zheng, F. An, Amphiphilic photosensitizer polymer as a nanocarrier of cytotoxic molecule for carrier-free combination therapy, MedComm-Biomaterials and Applications 2 (1) (2023) e28.

[7] M. Zhu, X. Yang, J. You, L. Zheng, C. Yi, Y. Huang, Nanobiotechnology-mediated radioimmunotherapy treatment for triple-negative breast cancer, MedComm-Biomaterials and Applications 2 (1) (2023) e32.

[8] Y. Li, Y. Dong, X. Zhou, K. Fan, Nanotechnology connecting copper metabolism and tumor therapy, MedComm-Biomaterials and Applications 2 (2) (2023) e36.

[9] L. Li, J. Yin, W. Ma, L. Tang, J. Zou, L. Yang, T. Du, Y. Zhao, L. Wang, Z. Yang, C. Fan, J. Chao, X. Chen, A DNA origami device spatially controls CD95 signalling to induce immune tolerance in rheumatoid arthritis, Nat. Mater. 23 (2024) 993–1001..

[10] Z. Wang, A. Jin, Z. Yang, W. Huang, Advanced nitric oxide generating nanomedicine for therapeutic applications, ACS Nano 17 (10) (2023) 8935–8965.

[11] X. Hu, Z. Fang, F. Sun, C. Zhu, M. Jia, X. Miao, L. Huang, W. Hu, Q. Fan, Z. Yang, W. Huang, Deciphering oxygen-independent augmented photodynamic oncotherapy by facilitating the separation of electron-hole pairs, Angew. Chem. 63 (15) (2024) e202401036.

[12] B. Wang, X. Hu, F. Sun, Z. Yang, W. Huang, Advanced strategic constructions of diketopyrrolopyrrole derivatives-based organic semiconducting phototheranostics, Interdisciplinary Medicine 1 (1) (2022) e20220010.

[13] G. Ge, Y. Zhang, X. Xiao, Y. Gong, C. Liu, C. Lyu, W.L. Ong, G.W. Ho, Z. Yang, W. Huang, Rapidly gelling, highly adhesive, and mechanically robust ionogels for stretchable and wireless electronics, Adv. Funct. Mater. 34 (21) (2024).

[14] W. Ma, H. Luo, J. Lv, P. Wen, G. Liu, Z. Yu, Z. Yang, W. Huang, Immunoregulatory engineering of semiconducting charge-reversal nanoantioxidant for ameliorating cancer radioimmunotheranostics, Adv. Mater. (2024) e2402929.

[15] S. Ning, M. Lyu, D. Zhu, J.W.Y. Lam, Q. Huang, T. Zhang, B.Z. Tang, Type-I AIE photosensitizer loaded biomimetic system boosting cuproptosis to inhibit breast cancer metastasis and rechallenge, ACS Nano 17 (11) (2023) 10206–10217.

[16] T. Zhang, J. Zhang, F.B. Wang, H. Cao, D. Zhu, X. Chen, C. Xu, X. Yang, W. Huang, Z. Wang, J. Wang, Z. He, Z. Zheng, J.W.Y. Lam, B.Z. Tang, Mitochondria-targeting phototheranostics by aggregation-induced NIR-II emission luminogens: modulating intramolecular motion by Electron acceptor engineering for multi-modal synergistic therapy, Adv. Funct. Mater. (2022) 2110526.

[17] D. Zhu, J. Zhang, G. Luo, Y. Duo, B.Z. Tang, Bright bacterium for hypoxia-tolerant photodynamic therapy against orthotopic colon tumors by an interventional method, Adv. Sci. 8 (15) (2021) 2004769.

[18] D. Zhu, Y. Duo, S. Meng, Y. Zhao, L. Xia, Z. Zheng, Y. Li, B.Z. Tang, Tumor-exocytosed exosome/aggregation-induced emission luminogen hybrid nanovesicles facilitate efficient tumor penetration and photodynamic therapy, Angew. Chem. 59 (2020) 2–10.

[19] Y. Duo, D. Zhu, X. Sun, M. Suo, Z. Zheng, W. Jiang, B.Z. Tang, Patient-derived microvesicles/AIE luminogen hybrid system for personalized sonodynamic cancer therapy in patient-derived xenograft models, Biomaterials 272 (2021) 120755.

[20] D. Zhu, T. Zhang, Y. Li, C. Huang, M. Suo, L. Xia, Y. Xu, G. Li, B.Z. Tang, Tumor-derived exosomes co-delivering aggregation-induced emission luminogens and proton pump inhibitors for tumor glutamine starvation therapy and enhanced type-I photodynamic therapy, Biomaterials 283 (2022) 121462.

[21] S. Ning, T. Zhang, M. Lyu, J.W.Y. Lam, D. Zhu, Q. Huang, B.Z. Tang, A type I AIE photosensitiser-loaded biomimetic nanosystem allowing precise depletion of cancer stem cells and prevention of cancer recurrence after radiotherapy, Biomaterials 295 (2023) 122034.

[22] H. Chen, X. Luo, Q. Huang, Z. Liu, M. Lyu, D. Chen, J. Mo, D. Zhu, Platelet membrane fusion liposome loaded with type I AIE photosensitizer to induce chemoresistance cancer pyroptosis and immunogenic cell death for enhancing cancer immunotherapy, Chem. Eng. J. 476 (2023) 146276.

[23] D. Zhu, Z. Zheng, G. Luo, M. Suo, X. Li, Y. Duo, B.Z. Tang, Single injection and multiple treatments: an injectable nanozyme hydrogel as AIEgen reservoir and release controller for efficient tumor therapy, Nano Today 37 (2021) 101091.

[24] T. Zhang, Z. Liu, W. Tang, D. Zhu, M. Lyu, J.W.Y. Lam, Q. Huang, B.Z. Tang, Mitochondria-targeting Type I AIE photosensitizer combined with H2S therapy: uninterrupted hydroxyl radical generation for enhancing tumor therapy, Nano Today 46 (2022) 101620.

[25] Y. Xiong, C. Xiao, Z. Li, X. Yang, Engineering nanomedicine for glutathione depletion-augmented cancer therapy, Chem. Soc. Rev. 50 (10) (2021) 6013–6041.

[26] B. Niu, K. Liao, Y. Zhou, T. Wen, G. Quan, X. Pan, C. Wu, Application of glutathione depletion in cancer therapy: enhanced ROS-based therapy, ferroptosis, and chemotherapy, Biomaterials 277 (2021) 121110.

[27] T.A. Mishchenko, I.V. Balalaeva, M.V. Vedunova, D.V. Krysko, Ferroptosis and photodynamic therapy synergism: enhancing anticancer treatment, Trends in cancer 7 (6) (2021) 484–487.

[28] A. Meister, M.E. Anderson, Glutathione, Annu. Rev. Biochem. 52 (1) (1983) 711–760.

[29] T. Yong, X. Zhang, N. Bie, H. Zhang, X. Zhang, F. Li, A. Hakeem, J. Hu, L. Gan, H. A. Santos, X. Yang, Tumor exosome-based nanoparticles are efficient drug carriers for chemotherapy, Nat. Commun. 10 (1) (2019) 3838.

[30] H. He, C. Guo, W. Liu, S. Chen, X.Y. Wang, H. Yang, Engineering nanostructured pure cancer cell membrane-derived vesicles as a novel therapeutic cancer vaccine, MedComm-Biomaterials and Applications 1 (2) (2022) e22.

[31] D. Wang, H. Su, R.T.K. Kwok, G. Shan, A.C.S. Leung, M.M.S. Lee, H.H.Y. Sung, I. D. Williams, J.W.Y. Lam, B.Z. Tang, Facile synthesis of red/NIR AIE luminogens with simple structures, bright emissions, and high photostabilities, and their applications for specific imaging of lipid droplets and image-guided photodynamic therapy, Adv. Funct. Mater. 27 (46) (2017).

[32] J. Wang, Y. Dong, Y. Li, W. Li, K. Cheng, Y. Qian, G. Xu, X. Zhang, L. Hu, P. Chen, W. Du, X. Feng, Y.-D. Zhao, Z. Zhang, B.-F. Liu, Designer exosomes for active targeted chemo-photothermal synergistic tumor therapy, Adv. Funct. Mater. 28 (18) (2018) 1707360.
[33] Z. Xie, X. Cai, C. Sun, S. Liang, S. Shao, S. Huang, Z. Cheng, M. Pang, B. Xing, A.A. A. Kheraif, J. Lin, O2-Loaded pH-responsive multifunctional nanodrug carrier for overcoming hypoxia and highly efficient chemo-photodynamic cancer therapy, Chem. Mater. 31 (2) (2019) 483–490.
[34] T. Luo, K. Ni, A. Culbert, G. Lan, Z. Li, X. Jiang, M. Kaufmann, W. Lin, Nanoscale metal-organic frameworks stabilize bacteriochlorins for type I and type II photodynamic therapy, J. Am. Chem. Soc. 142 (16) (2020) 7334–7339.
[35] S. Ning, M. Suo, Q. Huang, S. Gao, K. Qiao, M. Lyu, Q. Huang, T. Zhang, B.Z. Tang, Biomimetic fusion liposomes boosting antitumor immunity and promote memory T cell differentiation to inhibit postoperative recurrence of breast cancer, Nano Today 54 (2024) 102106.
[36] S. Ning, X. Zhang, M. Suo, M. Lyu, Y. Pan, Y. Jiang, H. Yang, J.W. Yip Lam, T. Zhang, L. Pan, B.Z. Tang, Platelet-derived exosomes hybrid liposomes facilitate uninterrupted singlet oxygen generation to enhance breast cancer immunotherapy, Cell Reports Physical Science 4 (7) (2023) 101505.
[37] X. Wang, Y. Liu, C. Xue, Y. Hu, Y. Zhao, K. Cai, M. Li, Z. Luo, A protein-based cGAS-STING nanoagonist enhances T cell-mediated anti-tumor immune responses, Nat. Commun. 13 (1) (2022).
[38] J. Lu, X. Liu, Y.P. Liao, X. Wang, A. Ahmed, W. Jiang, Y. Ji, H. Meng, A.E. Nel, Breast cancer chemo-immunotherapy through liposomal delivery of an immunogenic cell death stimulus plus interference in the Ido-1 pathway, ACS Nano 12 (11) (2018) 11041–11061.
[39] P. Zheng, B. Ding, Z. Jiang, W. Xu, G. Li, J. Ding, X. Chen, Ultrasound-Augmented mitochondrial calcium ion overload by calcium nanomodulator to induce immunogenic cell death, Nano Lett. 21 (5) (2021) 2088–2093.
[40] K. Wang, Y. Li, X. Wang, Z. Zhang, L. Cao, X. Fan, B. Wan, F. Liu, X. Zhang, Z. He, Y. Zhou, D. Wang, J. Sun, X. Chen, Gas therapy potentiates aggregation-induced emission luminogen-based photoimmunotherapy of poorly immunogenic tumors through cGAS-STING pathway activation, Nat. Commun. 14 (1) (2023) 2950.
[41] D.W. Zheng, F. Gao, Q. Cheng, P. Bao, X. Dong, J.X. Fan, W. Song, X. Zeng, S. X. Cheng, X.Z. Zhang, A vaccine-based nanosystem for initiating innate immunity and improving tumor immunotherapy, Nat. Commun. 11 (1) (2020) 1985.
[42] R. Song, T. Li, J. Ye, F. Sun, B. Hou, M. Saeed, J. Gao, Y. Wang, Q. Zhu, Z. Xu, H. Yu, Acidity-activatable dynamic nanoparticles boosting ferroptotic cell death for immunotherapy of cancer, Adv. Mater. 33 (31) (2021) e2101155.
[43] W. Fang, Z. Yu, P. Hu, J. Shi, Fe/Al-LDH nanomedicine for antitumor ferroptosis-immunotherapy by immunosuppression reversal, Adv. Funct. Mater. (2024) 2405483.
[44] Z. Zhou, H. Liang, R. Yang, Y. Yang, J. Dong, Y. Di, M. Sun, GSH depletion-induced activation of dimersomes for potentiating the ferroptosis and immunotherapy of "cold" tumor, Angew. Chem. 61 (2022) e202202843.
[45] D. Zhu, H. Chen, C. Huang, G. Li, X. Wang, W. Jiang, K. Fan, H_2O_2 self-producing single-atom nanozyme hydrogels as light-controlled oxidative stress amplifier for enhanced synergistic therapy by transforming “cold” tumors, Adv. Funct. Mater. 32 (16) (2022) 2110268.
[46] X. Sun, W. Sui, Z. Mu, S. Xie, J. Deng, S. Li, T. Seki, J. Wu, X. Jing, X. He, Y. Wang, X. Li, Y. Yang, P. Huang, M. Ge, Y. Cao, Mirabegron displays anticancer effects by globally browning adipose tissues, Nat. Commun. 14 (1) (2023) 7610.
[47] T. Tian, M. Heine, I. Evangelakos, M.Y. Jaeckstein, N. Schaltenberg, T. Stähler, F. Koch-Nolte, M. Kumari, J. Heeren, The P2X7 ion channel is dispensable for energy and metabolic homeostasis of white and brown adipose tissues, Purinergic Signal. 16 (4) (2020) 529–542.
[48] J. Huang, Z. Xiao, Y. An, S. Han, W. Wu, Y. Wang, Y. Guo, X. Shuai, Nanodrug with dual-sensitivity to tumor microenvironment for immuno-sonodynamic anti-cancer therapy, Biomaterials 269 (2021) 120636.